



Integrating experimental modeling techniques with the Pareto search algorithm for multiobjective optimization in the WEDM of Inconel 718

Mahmoud Hewidy¹ · Osama Salem¹

Received: 25 May 2023 / Accepted: 19 August 2023 / Published online: 13 September 2023
© The Author(s) 2023

Abstract

Inconel 718 is a superalloy with a high nickel content that is widely used in applications requiring solid mechanical behavior and resistance to oxidation and corrosion at high temperatures. This alloy has numerous applications in manufacturing steam turbine and jet aircraft interiors, aviation sector manifolds, and rotary spindles. It can be classified as a difficult-to-cut material unsuitable for traditional machining. The purpose of this paper is to develop prediction models for a wire electrical discharge machining (WEDM) process using response surface methodology (RSM), artificial neural networks (ANN), and adaptive neuro-fuzzy inference systems (ANFIS) and to determine which model is better at making accurate predictions. Pulse_ontime, pulse_offtime, servo voltage, flushing pressure, and wire feed were considered the main factors affecting volumetric material removal rate (VMRR) and arithmetic surface roughness (Ra), which were evaluated as WEDM performance characteristics. I-optimal design made with a computer algorithm was employed to develop experimental models. The results reveal that the wire feed and pulse_ontime were the most vital factors influencing VMRR, respectively, and the most significant factor influencing Ra is the pulse_ontime. The total percentage error of the three models demonstrated that the ANN and ANFIS models are more reliable and accurate than the RSM mathematical model. Finally, multiobjective optimization using the Pareto search algorithm was used to optimize mathematical, ANN, and ANFIS models to determine the optimum WEDM process parameters for machining Inconel 718 superalloy.

Keywords I-optimal design · Response surface methodology · Artificial neural network · Adaptive neuro fuzzy inference system

1 Introduction

The challenge of working with materials that are tough to cut was a significant factor in the development of advanced machining techniques; among such techniques is wire electrical discharge machining (WEDM), which is extensively used in the aircraft, automobile, and medical device industries [1]. Recently, (WEDM) has been used to machine various machining miniature and micro parts made from metallic, alloy, powdered, carbide, and ceramic materials [2]. Inconel 718 superalloy is a prevalent and extensively utilized nickel-based alloy. In 2019, Inconel 718 superalloy, comprising approximately 54% of the nickel superalloy market, was valued at over \$4 billion [3].

In 2021, the commercial aviation engine business was worth over \$80 billion. Inconel 718 superalloy, which constitutes over 50% of the total weight of these engines, has proven that this alloy is a significant contributor to this market [4].

The precipitate strengthening process and the distribution of the particles of chrome and iron, niobium, molybdenum, titanium, and aluminum throughout the nickel γ matrix allow Inconel 718 to retain its mechanical characteristics even at 650 degrees Celsius [5]. This lead Inconel 718 is utilized significantly in various applications, such as the interiors of steam turbines and jet aircraft, and rotary spindles [6]. Cutting Inconel 718 superalloy using conventional machining techniques is problematic, due to high cutting forces with generated stresses exceeding $450 * 10^6$ Pa and temperature exceeding 1100 degrees Celsius on the cutter's edge. These issues shorten the cutter edge's lifespan, which increases expenses [7]. The challenges of cutting hard materials can be reduced to a manageable level using (WEDM). However, choosing the appropriate machining settings for this process,

✉ Osama Salem
Osama.Mohammed@sh-eng.menofia.edu.eg

¹ Department of Production Engineering and Mechanical Design, Faculty of Engineering, Minufiya University, Shebin El-Kom, Egypt

which are controlled by several primary and secondary factors like peak current, pulse_ontime, pulse_offtime, servo voltage, wire tension, gap voltage, Arc ontime, Arc offtime, Flushing Pressure, wire feed, and thermo-mechanical properties of the workpiece and electrode wire for the necessary performance characteristics of (WEDM) process machining such as the volumetric material removal rate (VMRR), arithmetic surface roughness (Ra), kerf width (KW), and others, has always been one of the industry's most complex challenges.

2 Literature review

Many research have been made to improve the performance characteristics of the WEDM process, such as (VMRR), (Ra), and (KW), by using a wide range of traditional multi-criteria-making decisions and evolutionary optimization techniques. Nevertheless, due to the complexity and stochasticity of the process and the inclusion of many factors, its full capabilities have yet to be discovered; besides that, finding a reasonably accurate relationship function between the performance characteristics and process parameters is hard. Aggarwal et al. [8] developed a mathematical model using RSM to predict, with an error of less than 5%, the cutting rate, and the (Ra) by WEDM when machining Inconel 718 superalloy with different operating settings (peak current, pulse_ontime, pulse_offtime, wire tension, gap voltage, and wire feed). Cutting rate and (Ra) were improved to 2.55 mm/min and 2.54 μm , respectively, using multi-response optimization to determine the best machining settings. Yusoff et al. [9] developed a model called OrthoANN that was created by combining the Taguchi design orthogonal array technique L256 with an artificial neural network (cascade forward back propagation neural network (CFNN)). This model was successful in predicting the performance characteristics (cutting speed, Ra, VMRR, and sparking gap) with an average error of 5.16% while machining Inconel 718 superalloy under varying operating settings such as (peak current, pulse_ontime, pulse_offtime, servo voltage, and flushing Pressure), demonstrating the effectiveness of OrthoANN in modeling the performance characteristics of the WEDM on Inconel 718 superalloy compared to conventional ANN. Lalwani et al. [10] utilized two models, first a mathematical model using the RSM and second the ANN model, to predict the (Ra), the (KW), and the (VMRR) by WEDM while machining Inconel 718 superalloy under varying operating settings (pulse_ontime, pulse_offtime, servo voltage, and wire tension), and concluded that the prediction accuracy of the established ANN model was found to be superior to the RSM model. The lower value of the mean square error for ANN (1.49%) than the mean square error for RSM (5.71%), which further validates the better fitting of the neural network, otherwise

indicates that (pulse_ontime) has the highest impact on the machining of Inconel 718 superalloy by the WEDM process. Ultimately, the non-dominant sorting genetic algorithm (NSGA-II) used multiple objectives to find the best WEDM conditions. Lijun Liu et al. [11] attempted to use a zinc-diffused-coated brass wire electrode and the Taguchi-Data Envelopment Analysis-based Ranking (DEAR) methodology while machining Inconel 718 superalloy under varying operating settings (pulse_ontime), (pulse_offtime), (Servo Voltage), and (wire tension) to improve the WEDM process' performance characteristics ((Ra), (VMRR), and (KW)) and proposed that the ideal input factor configuration discovered in WEDM be 140 μs (pulse_ontime), 50 μs (pulse_offtime), 60 Volt (Servo Voltage), and 5 kg (wire tension), with an error accuracy of 1.1%. Finally, state that the (pulse_offtime) is the most important factor influencing the average surface roughness due to its importance in deionization in the machining process. Wan Azhar et al. [12] utilized a model that considers material properties such as thermal conductivity, melting point, and electrical resistivity. Coactive Neuro-Fuzzy Inference Systems (CANFIS) is a promising method to model the μEDM performances on different materials to predict the material removal rate (MRR), total discharge pulse, overcut, and taperness under variable input parameters. The material properties, feed rate, capacitance, and gap voltage are in a three-level design based on a full factorial experiment, and it was determined that the mean average percentage error of various outputs for test datasets, including MRR, total discharge pulse, overcut, and taper angle, was 4.5%, 6.8%, 15.4%, and 15.2% respectively. Biswas et al. [13] used genetic algorithms (GAs) and particle swarm optimization (PSOs) to make models of multiobjective, multilayer neural networks (MOMLNNs). To discover effective methods for optimizing multimaterial systems, the MOMLNN with the (13–300–300–4) architecture was paired with GA and PSO techniques to discover the ideal process parameters by the WEDM for machining Inconel 625 and Inconel 718 superalloy. Six process parameters (pulse_ontime, pulse_offtime, servo voltage, Arc ontime, Arc offtime, and wire feed), seven elements (Fe, Nb, Cr, Mo, Al, Si, and Ti), and four performance characteristics of the WEDM process ((VMRR), (KW), (Ra), and recast layer thickness (RLT)) make up this model. When comparing GA and PSO integrated models, GA has somewhat higher accuracy. It concludes that the (VMRR) and (KW) increase when pulse_ontime and Arc ontime increase. (Ra) decreases when Arc ontime and wire feed decrease. As Arc offtime increases, so does the recast layer's thickness (RLT). The alloying elements most significantly impacting VMRR, KW, and Ra are Cr, Mo, and Si, while Fe, Nb, Ti, and Al mainly govern the RLT. Finally, the error fraction between the optimal and experimental answers was often less than 5%, showing that the GA-integrated model has strong predictive accuracy.

This literature review highlighted the significant work produced over the past few years by numerous authors in machining Inconel 718 superalloy. This review gives our study some direction and introduces path analysis as a valuable tool to model the relationships between various WEDM process parameters and performance characteristics. According to the literature review cited above, none of the authors used the I-optimal design of mixture experiments when creating the experimental design for the WEDM process. Additionally, only a few studies have employed multi-response optimization strategies for the ANN and ANFIS models of the WEDM process of Inconel 718 superalloy. Almost all authors have utilized coded values for input process parameters, resulting in more intricate and challenging models to implement in industrial settings.

This study aims to construct a predictive model using actual values of processing parameters (pulse_ontime, pulse_offtime, servo voltage, Flushing Pressure, and wire feed) to make it more realistic and valuable for machining the Inconel 718 superalloy by the wire electrical discharge cutting process. The experimental design for the WEDM process will use an I-optimal design of mixture experiments to make accurate mathematical, ANN, and ANFIS models that can predict performance characteristics ((VMRR) and (Ra)). By using the percentage error and regression analysis, it will determine which model is more reliable and accurate than the others. A parametric analysis will investigate the impact of input processing parameters on performance characteristics such as (VMRR) and SR. The performance of the WEDM process will be optimized using the Pareto search algorithm to the mathematical, ANN, and ANFIS models.

3 Experimental procedures

3.1 Specimen material

Inconel 718 superalloy was the material of the specimen tested in this experiment (16 mm in diameter). The combination of chemical elements in the workpiece specimen is displayed in Table 1. It has a density of 8.32401 g/cm³ and a melting temperature that ranges from 1210 to 1344 °C.

3.2 Experimental setup

The WEDM process’ schematic design and the initial setup are seen in Figs. 1 and 2, respectively. There are 32 experiments in Fig. 3 carried out on an ACCUTEX AU-500IA CNC as shown in Fig. 4 (with other experimental details). These experiments were performed by generating a pulsed spark between a wire made of uncoated brass CuZn377 with a diameter of 0.25 mm and an Inconel 718 superalloy specimen (16 mm in diameter).

Table 2 provides an overview of all the machining settings.

Most CNC wire EDM machines cannot determine optimal process parameters for various workpiece materials, even though this information is essential in the precise manufacturing business. Basic materials, including steel, aluminum, and carbides, are listed in the commercial WEDM machine catalog. However, WEDM is required to process various materials because of their unique thermophysical characteristics. Each workpiece material, such as Inconel 718 superalloy, requires the machine’s end user to conduct

Table 1 Workpiece chemical composition (wt%)

Element	Weight	Element	Weight	Element	Weight	Element	Weight
Ni	55.4	Fe	17.7	V	0.0622	Mg	0.0013
Si	0.139	Co	0.136	C	0.0312	Ta	0.0025
Mn	0.183	Ti	1.49	P	0.0040	Zr	0.0010
Cr	16.9	Al	0.612	S	0.0003	B	0.0048
Mo	2.17	Nb	4.60	Sn	0.0049	N	0.305
Cu	0.0802	W	0.0372	Hf	0.0856	Pb	0.0317

Fig. 1 WEDM process’ schematic design

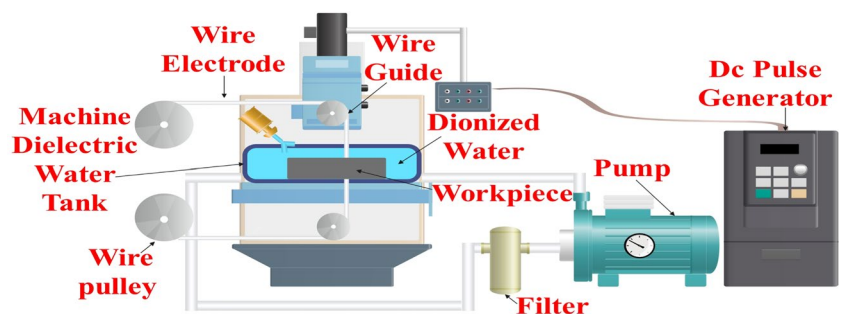




Fig. 2 Initial setup

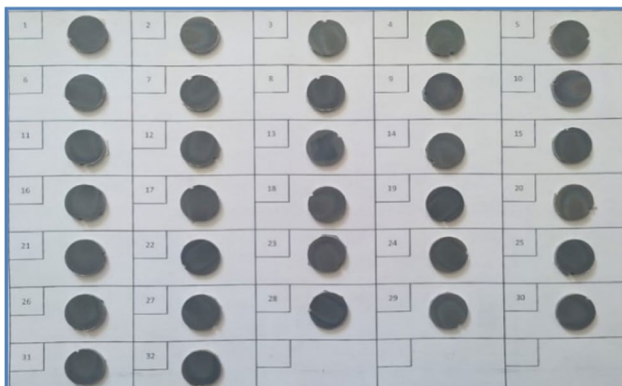


Fig. 3 32 samples cutting on wire EDM machine

time-consuming experiments to determine the best process settings. This paper studies the WEDM performance of Inconel 718 superalloy utilizing uncoated brass wire and analyzes the impact of process parameters ((Pulse_ontime), (Pulse_offtime), (Servo Voltage), (Flushing Pressure), and (wire feed)) on the responses (VMRR) and the (Ra). The is specified using the following equation:

$$\text{VMRR (mm}^3/\text{min)} = \frac{(\text{sample weight prior to machining (gm)} - \text{sample weight following machining (gm)})}{\text{Density of Inconel 718 superalloy (gm/cm}^3) * 1000 * \text{Machining time (min)}} \quad (1)$$

Therefore, this method yields lower standard errors, more accuracy, and higher accuracy for predicting. Third, unlike traditional RSM, the I-optimal method may match complicated empirical regression models. The I-optimal method is used to solve issues with numerous constraints. For example, the levels of parameters are limited to specified values or a variable number of levels within parameters. This is done

A highly accurate electrical balance, capable of measuring with a resolution of 0.1 mg, is utilized to determine the weight of the specimen both before and after the machining process. To determine the effect of WEDM processing parameters on the machinable surface, each specimen's (Ra) is measured with a surface roughness meter (TR210, Beijing). Using a surface roughness meter, Ra was measured in three distinct locations on the same face, and the average of those three readings was taken as the actual Ra value. The indicator has been set to the following parameters: the digital filter (RC) and the cut-off length (λ_c) (0.8 mm). Finally, scanning electronic microscopic pictures with a microscope (JSM-6390 series, Japan) was used to analyze the surface topography and shed light on the surface roughness.

4 Design of experiments

The RSM technique is a statistical technique that may be used to model, analyze, and optimize problems when the interaction of the input factors influences the output response to be studied because of its efficiency and adaptability. The I-optimal design of mixture experiments can characterize and optimize a process with great precision. In this experiment, an I-optimal design made with a computer algorithm is used to improve the accuracy of predictions across the design space [14]. There are several benefits to using an I-optimal design instead of a traditional (RSM) design. First, fewer runs are needed than in traditional RSM approaches. For example, an experiment with five factors that use usual (RSM) approaches must have 50 trials with the central composite design (CCD) and 46 runs with the Box Behnken design (BBX) without duplicating the design runs in order to improve the accuracy of predictions. On the other hand, the I-optimal design of mixture experiments requires just 21 trials and a small number of duplicated design points. Also, the I-optimal design is a custom criterion that usually leads to a more even spread of design points in extreme regions.

by taking out a specific area of study where responses could not be evaluated well (e.g., in WEDM parameters optimization) [15]. There were 32 trials in the I-optimal model matrix displayed in the table. The table below is an I-optimal model matrix consisting of 32 trials, 21 of which were for the basic model, 7 for extra model points in support of this model, 3 for estimating lack of fit, and 1 for replications. The

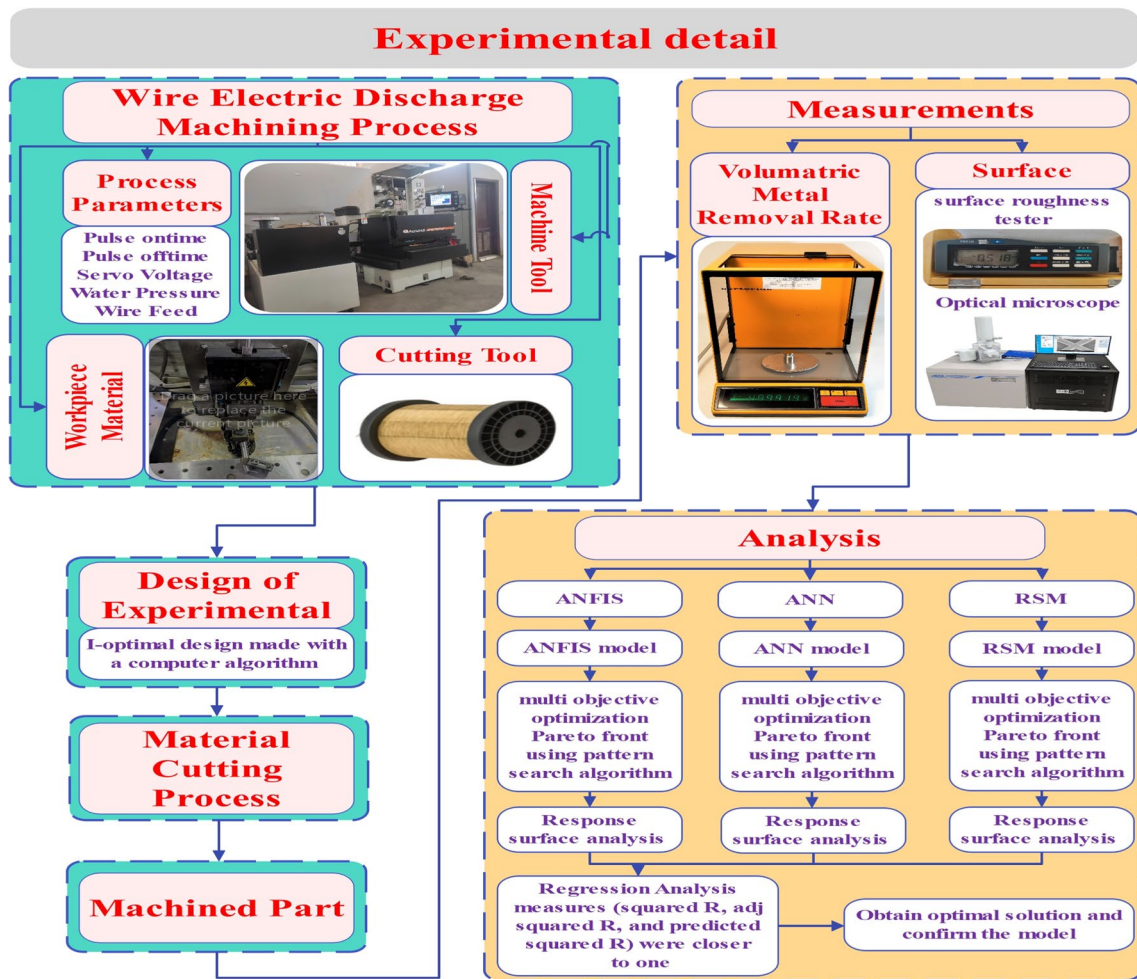


Fig. 4 Experimental details and framework

process parameters at different levels are displayed in the Table 3. All statistics from the experiments were analyzed using Design Expert software. Table 4 displays the outcomes of the experiment.

5 Results and discussion

5.1 Prediction and modeling for (VMRR) and (Ra) using response surface methodology

The response surface technique is a way to figure out the relationship between the output response to be studied and the input factors (process parameters of WEDM) and how these factors affect the responses [14]. In order to investigate the impact that WEDM processing parameters have on the (VMRR) and (Ra) when machining Inconel 718 superalloy, a second-order polynomial response can be included in the following equation:

Table 2 Wire electrical discharge machine operating conditions

Parameters	Description
Wire polarity	Positive
Wire material	Brass (Cu_Zn_377)
Wire diameter (mm)	0.25
Open voltage (volt)	82
Pulse-ontime (nanosecond)	(250 – 750)
Pulse-offtime (microsecond)	(10 – 20)
Arc ontime (nanosecond)	(Pulse_ontime – 50 n.s)
Arc offtime (microsecond)	(Pulse_offtime + 2 μ.s)
Servo voltage (volt)	(35 – 55)
Flushing pressure (bar)	(4.00—6.50)
Wire feed (mm/second)	(1.00 – 3.00)
Wire tension (gf)	(1400)
Wire-speed (mm/second)	80
Water level (litre)	80
Dielectric fluid	De-ionized water including (de-ionizing agent zeolite)
Water resistance kΩ.cm	17
Peak current (A)	Determined by the machine itself based on the parameter of the feeding rate

Table 3 Selected input parameters and their levels

Input Param- eters	Units	L [1]	L [2]	L [3]	L [4]	L [5]	L [6]	L [7]	L [8]	L [9]	L [10]	L [11]	L [12]	L [13]	L [14]	L [15]	L [16]	L [17]	L [18]	L [19]	L [20]		
(Pulse-ontime)	Nano Second	11	250	300	350	400	450	500	550	600	650	700	750	-	-	-	-	-	-	-	-	-	
(Pulse-offtime)	Micro Second	11	10	11	12	13	14	15	16	17	18	19	20	-	-	-	-	-	-	-	-	-	
(Servo volt- age)	Volt	21	35	36	37	38	39	40	41	42	43	44	45	46	47	48	49	50	51	52	53	54	55
(Flushing pres- sure)	Bar	3	4	5	6.5	-	-	-	-	-	-	-	-	-	-	-	-	-	-	-	-	-	-
(Wire feed)	mm/sec	21	1	1.1	1.2	1.3	1.4	1.5	1.6	1.7	1.8	1.9	2	2.1	2.2	2.3	2.4	2.5	2.6	2.7	2.8	2.9	3

$$\begin{aligned}
 \text{Predicted Response} = & x(0) + x(1)a + x(2)b + x(3)c + x(4)d + x(4)e + x(12)ab \\
 & + x(13)ac + x(14)ad + x(15)ae + x(23)bc + x(24)bd + x(25)be \\
 & + x(34)cd + x(35)ce + x(45)de + x(11)a^2 + x(22)b^2 + x(33)c^2 \\
 & + x(44)d^2 + x(55)e^2 \pm \epsilon
 \end{aligned}
 \tag{2}$$

where,
 x (0) is the free term.
 a; b; c; d; and e are values of the machining process parameters.
 x (1); x (2); x (3); x (4); and x (5) are values of linear coefficients.
 x (12); x (13); x (14); x (15); x (23); x (24); x (25); x (34); x (35); and x (45) are values of interaction coefficients.
 x (11); x (22); x (33); x (44); and x (55) are values of squared coefficients.
 ε is the fitting error of the uth observation + 0.000075.
 The final response equations were formulated using multiple regression analysis for the (VMRR) and (Ra).

$$\begin{aligned}
 \text{VMRR} = & (2.6507457 - 0.000217128 * T_{on} - 0.288503 * T_{off} \\
 & + 0.2066369 * S.V - 0.9456873 * P + 0.5724595 \\
 & * W.F + 7.46812191 * 10^{-05} * T_{on} * T_{off} + 0.000532204 \\
 & * T_{on} * P + 0.00183019 * T_{on} * W.F - 0.003000084 \\
 & * T_{off} * S.V + 0.007696312 * S.V * P + 0.10160268 \\
 & * P * W.F - 5.3301719 * 10^{-06} * T_{on}^2 + 0.0131177350 \\
 & * T_{off}^2 - 0.002187750 * S.V^2 - 0.3338437703 * W.F^2)^2
 \end{aligned}
 \tag{3}$$

In the VMRR equation, using a transformer for linear regression with the square root makes the determination factor (R^2) and prediction (R^2) larger, which supports this model.

$$\begin{aligned}
 \text{Ra} = & (-0.083028455 + 0.0015128181 * T_{on} + 0.070355985 * T_{off} \\
 & + 0.050550919 * S.V - 0.19759415 * P - 0.37672159 * W.F \\
 & - 7.206721 * 10^{-05} * T_{on} * T_{off} + 0.002884426 * T_{on} * W.F \\
 & - 0.0020588609 * T_{off} * S.V + 0.003541168 * S.V * P \\
 & + 0.0049794922 * S.V * W.F + 0.002147321 * T_{off}^2 \\
 & - 0.00051503584 * S.V^2)
 \end{aligned}
 \tag{4}$$

where T_{on} (n.s), T_{off} (μ.s), S.V (volt), P (bar), and W.F (mm/second) are (Pulse-ontime), (Pulse-offtime), (Servo Voltage), (Flushing Pressure), and (Wire feed) respectively.

Design of Expert 13 and Minitab 21 were used to test the models' adequacy using ANOVA. Nominal model terms were eliminated using backward elimination. In this experiment, all of the adequacy measures (squared R, adj squared R, and predicted squared R) were closer to one, suggesting that the model was adequate and fit. The R^2 value for VMRR is 97.34%, and Ra is 89.87%. The high adj R^2 and predicted R^2 values, 94.61% and 92.29% for VMRR and 83.47% and

Table 4 Design of experiments matrix and results

Exp.no	(Pulse-ontime) (n.s)	(Pulse-off-time) (μ.s)	(Servo voltage) (volt)	(Flushing pressure) (bar)	(Wire feed) (mm/second)	VMRR (mm ³ /min)	Ra (μ.m)
1	450	17	47	6.5	1	3.64848	1.274
2	750	20	49	5	1.6	8.59081	1.55367
3	600	10	41	5	1	4.50864	1.48267
4	700	12	45	5	2	9.0293	1.389
5	750	18	35	4	1	4.17707	1.56467
6	250	17	55	5	2.4	3.88995	1.01
7	450	10	47	6.5	2.4	10.6475	1.3
8	550	20	43	4	3	13.8227	1.293
9	250	19	35	4	2.7	6.3455	1.388
10	750	10	55	5	1	4.51585	1.569
11	350	12	50	5	2.6	10.4865	1.22
12	400	20	35	5	1.6	7.34502	1.351
13	400	13	35	5	3	6.62061	0.92
14	750	13	49	5	3	14.6804	1.701
15	250	14	42	4	1.8	6.3467	1.10767
16	250	10	55	5	1	4.04252	1.09533
17	250	20	55	5	1	3.33493	1.09333
18	750	16	35	6.5	2.2	9.58192	1.384
19	250	10	35	5	1	3.43224	0.934
20	650	20	35	6.5	1	4.53387	1.46467
21	750	19	55	4	2.7	13.1631	1.55867
22	250	10	55	5	3	5.49254	0.958333
23	650	20	55	6.5	3	16.1641	1.394
24	250	14	42	4	1.8	6.64343	0.999333
25	550	13	45	5	2.3	11.4068	1.40967
26	600	16	50	4	2.6	12.4495	1.511
27	250	17	55	6.5	2.4	3.91518	0.961333
28	250	20	39	6.5	3	4.51345	1.05433
29	600	14	55	4	1.8	7.44953	1.37267
30	750	10	35	4	2.6	12.1852	1.621
31	600	15	44	6.5	1.5	5.06847	1.30667
32	750	15	52	6.5	3	15.8085	1.66067

72.7% for Ra as shown in Fig. 5, demonstrate the validity of these models. Both predicted R^2 and modified R^2 were found to be consistent. Lack of fit was deemed non-significant in each case, as needed. The 95% confidence level was used to find the significant machining factors that impact the response variables, namely VMRR and Ra. As seen in Fig. 6, the (wire feed) has the highest contribution percentage to (VMRR), with a contribution percentage of 50.67%. This implies that the (wire feed) in which the wire is fed into the workpiece

significantly impacts the VMRR due to an increase in consumed applied current, which increases the heat energy rate and, thus, the melting and evaporation rate [16]. Furthermore, (pulse_ontime) has a significant contribution percentage of 30.67%. This indicates that the pulse duration significantly impacts the VMRR because increased discharge energy melts more material from the workpiece [17]. Furthermore, the “water pressure” parameter has a contribution percentage of 2.43%, indicating that the WEDM machine’s water pressure

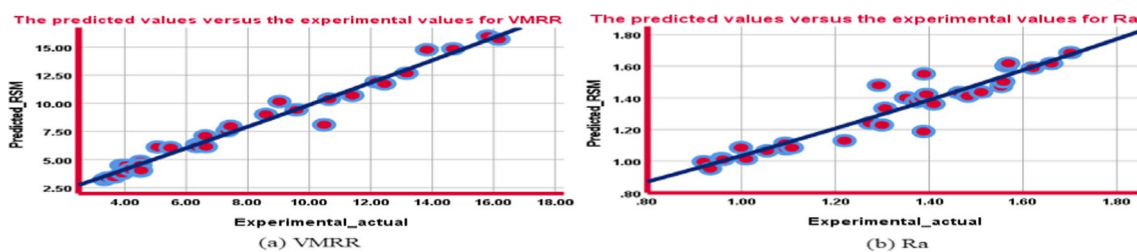


Fig. 5 The predicted values versus the experimental values for **a** VMRR and **b** Ra of the mathematical model (RSM)

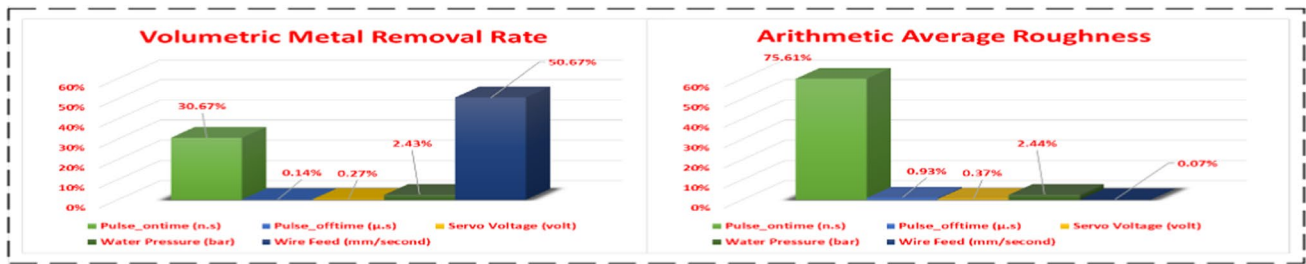


Fig. 6 Percentage contribution of WEDM input parameters in controlling the performance characteristics (VMRR and Ra)

has a minor effect on the VMRR. Furthermore, the (Servo Voltage) and (pulse_offtime) contribute 0.27% and 0.14%, respectively, indicating that these factors have a smaller impact on VMRR. Finally, the wire feed rate and pulse on time are the most influential factors on the VMRR of the wire EDM machine. These parameters must be optimized to maximize the efficiency and effectiveness of the WEDM process, and it was found that the (pulse_ontime) has the highest percentage contribution (75.61%) to the arithmetic surface roughness (Ra). This implies that changing the (pulse_ontime) can significantly impact the surface roughness. Increased (pulse_ontime) causes increased spark intensity and increases the size of the craters on the machine surface, resulting in poor surface quality [10]. On the other hand, contribution percentages for (pulse_offtime, servo voltage, Flushing Pressure, and wire feed) are relatively low (0.93%, 0.37%, 2.44%, and 0.07%, respectively). This means that these factors have a minor impact on surface roughness than (pulse_ontime). However, it is important to note that even minor changes in these parameters can affect surface roughness.

5.2 Prediction modeling for (VMRR) and (Ra) using artificial neural networks

The artificial neural network is a machine learning technique that employs neural networks to derive a continuous output variable from discrete input variables. It is a powerful tool for modeling complex, nonlinear relationships and can be applied to various disciplines, including finance, economics, engineering, and more. There are two principal types of artificial neural

networks (ANNs): feed-forward backpropagation and recurrent neural networks. Backpropagation feed-forward neural networks are the most common type and consist of layers of neurons that process input data and generate output. In contrast, recurrent neural networks are designed to process sequential data and have loops that allow information to travel through the network multiple times. Both types of ANNs have advantages and can be used depending on the problem and data set [18]. The ANN architecture was designed using MATLAB R2022b software in this experiment. The input layer is associated with (pulse_ontime, pulse_offtime, servo voltage, Flushing Pressure, and wire feed). The output layer is proportional to the (VMRR) and the (Ra). The hidden layer of neurons is connected to the input layer to the output layers as shown in Fig. 7. The ANN models for the (VMRR) and the (Ra) were created after extensive testing and use of the network. The ANN model feed-forward back propagation neural network with a 5–10–2 structure with the learning algorithm Bayesian regularization (BR), data split into 15% test data and 85% training data, was used to predict WEDM attributes. The correlation coefficient (R) value for VMRR and Ra in the present neural network model is 0.9996%. From a statistical standpoint, a network may properly compare input and output properties if the coefficient correlation is close to 1. This demonstrates that the measured and predicted values of VMRR and Ra using a feed-forward backpropagation neural network (FFBP) agree. Finally, using SPSS Statistical 27 for running regression tests on predicted and experimental data to compare to other predicted models, the R^2 value for VMRR is 99.72%, and Ra is 94.77% as shown in Fig. 8. The adj R^2 and predicted R^2 values for VMRR are

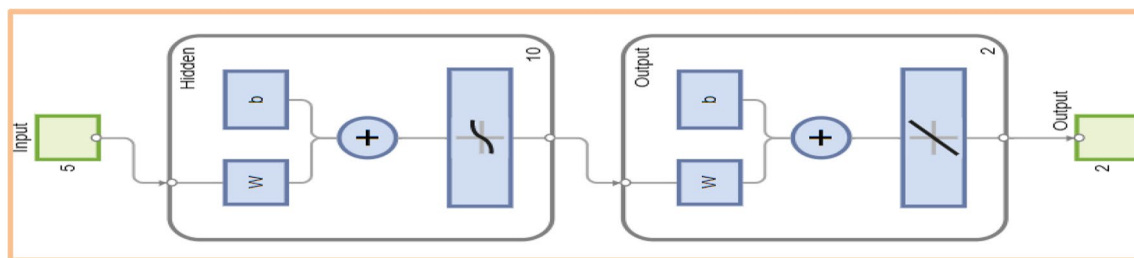


Fig. 7 The Structure of using artificial neural network

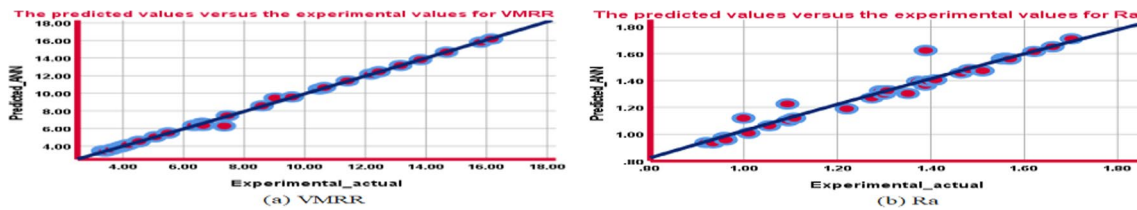


Fig. 8 The predicted values versus the experimental values for a VMRR and b Ra of the ANN model

99.71% and 99.7%, respectively, while the values for Ra are 94.59% and 94.23%.

5.3 Prediction modelling for (VMRR) and (Ra) using adaptive neuro-fuzzy model

ANFIS is a hybrid guessing model that uses neural networks and fuzzy logic to create a mapping between inputs and outputs. In the hybrid technique, the neural network is trained with data, while fuzzy logic is based on language rules called “if-then rules.” If the rules are combined with training data, the system generated is known as a fuzzy inference system, which is the most crucial soft computing technique [19]. Here, the ANFIS method was employed to establish a connection between the various inputs of the process (pulse_ontime, pulse_offtime, servo voltage, Flushing Pressure, and wire feed) and the most important performance characteristics ((VMRR) and (Ra)). It follows that a unique ANFIS model could be created for every output as seen in Fig. 9. For instance, to predict the (VMRR) and (Ra), two models represent the first layer of the ANFIS structure, the input layer, which has five nodes. The output layer contains a single node representing the first model’s (VMRR) values and the (Ra) for the second model. With the help of this method, a map is established between the process inputs and the (VMRR) and (Ra). The ANFIS toolbox, available in MATLAB R2022b, was used for this purpose. The prediction of (VMRR) and (Ra) by ANIFS has two basic steps: training and testing. Therefore, the ANFIS network has been trained using the 27 data sets. After training, the network was tested using the remaining five data

sets. The accuracy of ANFIS predictions depends on several factors, such as the type of fuzzy-based rule, the number of membership functions (MFs), and the type of membership functions. The paper’s prediction model was built using a first-order TSK-type fuzzy-based rule. Then, several iterations with different membership function numbers were attempted. The RMSE error objective was set to 0, and the number of iterations was 30, so all possible networks could be compared and the most accurate one chosen. In other words, the training epochs will continue until the RMSE is less than 0 or the epoch count reaches 30. Since the same RMSE metric is used to evaluate all networks, their performance can be compared. By trying out different ANFIS model structures for each response ((VMRR) and (Ra)), it was found that structures with 11 membership functions (2–2–3–2–2 topography) had the lowest root-mean-square deviation (RMSE) value. The selection of membership functions can also affect the ANFIS model’s precision. Several different membership functions (MFs), including triangular, trapezoidal, modified bell, and Gaussian, can be used and give the lowest root-mean-square deviation (RMSE) value that can be chosen. Training has been completed on the 2–2–3–2–2 structure with Gaussian membership functions. Root-mean-square deviation (RMSE) has been determined for VMRR, 0.00010736 and 0.78252 for training and test data, respectively, and Ra 8.3397×10^{-06} and 0.06484 for training and test data, respectively. Finally, using IBM SPSS Statistical 27 for running regression tests on predicted and experimental data to compare to other predicted models, the R^2 value for VMRR is 99.48%, and Ra is 98.68% as shown in Fig. 10. The adj R^2 and predicted R^2 values

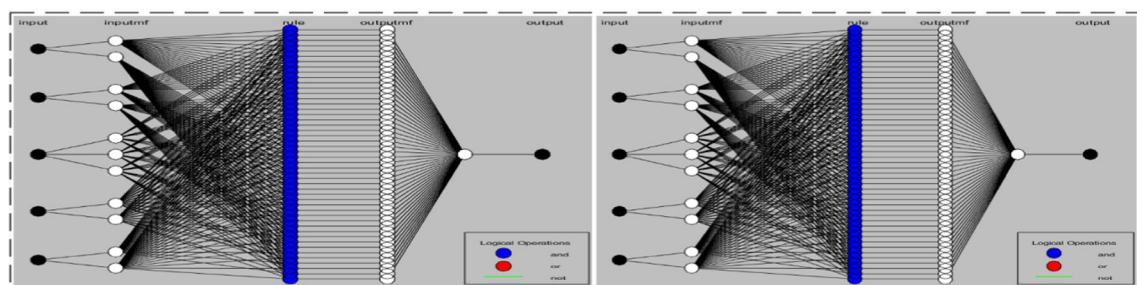


Fig. 9 The structure of using the ANFIS model for a VMRR and b Ra



Fig. 10 The predicted values versus the experimental values for a VMRR and b Ra of the ANFIS model

for VMRR are 99.46% and 97.96%, respectively, while the values for Ra are 98.59% and 97.84%.

5.4 Comparison of response surface methodology, artificial neural networks and adaptive neuro-fuzzy mode

Based on the work of Hasan M Saleh et al. [20], the analysis method employed to justify the findings in Table 5, which presents the results of a study comparing the performance of three different prediction models (RSM, ANN, and ANFIS) with their respective performance metrics ((the total percentage error: represents the percentage difference between the predicted results and the actual values obtained from experiments), (R^2 indicates the proportion of variance in the data that is accounted for by the model), (adj R^2 taking into account the number of predictors in the model), and (predicted R^2 indicating how well the model predicts new data)) for predicting two variables: (VMRR) and (Ra). For the VMRR predictions, the RSM model yielded a predicted value with a total percentage error of 6.39%. On the other hand, the ANN and ANFIS models produced more accurate predictions, with total percentage errors of 0.87% and 1.54%, respectively. These low errors percentage indicate that the ANN and ANFIS models performed well in predicting the VMRR values. However, for Ra predictions, the RSM model predicts Ra with an error of 4.30%, while the ANN and ANFIS models show lower percentage errors of 2.11% and 1.07%, respectively. This indicates that the ANN and ANFIS models provide more accurate Ra predictions than the RSM model. The R^2 values for VMRR, all three models show relatively high values, indicating that they can explain a significant proportion of the variance in the data. The ANN

model has the highest R-sq value (99.72%), followed by the ANFIS model (99.48%) and the RSM model (97.34%). These prove that the ANN and ANFIS models captured a significant portion of the variance in the VMRR values. For Ra, the R^2 values for the RSM, ANN, and ANFIS models are 89.87%, 94.77%, and 98.68%, respectively. These values suggest that the ANFIS model has the highest level of accuracy in predicting Ra, followed by ANN. The RSM model has the lowest level of accuracy in this regard. Additionally, for VMRR, the RSM model’s adj R^2 value is 94.61%, while the ANN and ANFIS models have adj R^2 values of 99.71% and 99.46%, respectively. These values suggest that the ANN and ANFIS models have higher predictability and are less prone to overfitting than the RSM model, but for Ra, the adj R^2 values for the RSM, ANN, and ANFIS models are 83.74%, 94.59%, and 98.59%, respectively, and these lead to the conclusion that the ANFIS model demonstrates the highest level of accuracy, while the RSM model shows the lowest level. Lastly, looking at the predicted R^2 values for VMRR, the ANN model performs the best (99.70%), followed by the ANFIS model (97.96%) and the RSM model (92.29%). These values indicate how well the models are expected to perform on new data. However, for Ra, the predicted R^2 values for the RSM, ANN, and ANFIS models are 72.70%, 94.23%, and 97.84%, respectively. Prove that the ANFIS model outperforms the others in terms of predictive ability. The results show that the ANN and ANFIS models outperform the RSM model in predicting both VMRR and Ra. The ANN model has the lowest total percentage error for VMRR predictions, while the ANFIS model has the lowest percentage error for Ra predictions. Additionally, both the ANN and ANFIS models have higher R^2 values, indicating that they can explain a significant proportion of the variance

Table 5 The percentage error and regression analysis for RSM, ANN, and ANFIS models

	Predicted (Rsm)		Predicted (ANN)		Predicted (ANFIS)	
	VMRR	Ra	VMRR	Ra	VMRR	Ra
Total percentage error	6.387%	4.301%	0.8738%	2.111%	1.539%	1.069%
R^2	97.34%	89.87%	99.72%	94.77%	99.48%	98.68%
Adj R^2	94.61%	83.74%	99.71%	94.59%	99.46%	98.59%
Predicted R^2	92.29%	72.70%	99.70%	94.23%	97.96%	97.84%

in the data. The ANN model also performs best regarding adj R^2 and predicted R^2 values for VMRR, while the ANFIS model has the highest accuracy in predicting Ra. Overall, it was determined that the ANN and ANFIS models are more reliable and accurate than the RSM model.

5.5 Response surface analysis of VMRR and Ra using an ANN model

The parametric analysis has been carried out to study the influences on performance characteristics such as (VMRR) and (Ra) by processing parameters (pulse_ontime, pulse_offtime, servo voltage, Flushing Pressure, and wire feed). Three-dimensional responses surface plots were created using the ANN model with NCSS 2021 software. In contrast, all previous studies used mathematical and ANFIS models to evaluate the change in the response surface. These surfaces further explained the relationship between the input process parameters and responses and demonstrated that the ANN model could estimate the (VMRR) and (Ra).

5.5.1 The ANN surfaces of the (VMRR) for the interaction terms

The response surface of (VMRR) versus (pulse_ontime) and (pulse_offtime) (hold values: (Servo Voltage) = 45 V (Flushing Pressure) = 5.25 bar (wire feed) = 2 mm/second) is presented in Fig. 11.

From this Fig. 11, it was observed that the VMRR increased with an increase in (pulse_ontime) value due to an increase in the discharge energy melting more material from the workpiece, thus increasing the VMRR values. Additionally, a higher (pulse_ontime) means maintaining the high heating temperatures for longer [17].

However, when (pulse_offtime) was low, it was found that increasing (pulse_ontime) at a specific value did not change VMRR because there was not enough time to flush

the molten material. At low (pulse_ontime), it was observed that the VMRR decreased with an increase in (pulse_offtime) due to more time passing between two successive electrical discharges [10], as seen from Fig. 11, but at high (pulse_ontime), it was found that the (pulse_offtime) did not much influence the VMRR.

The response surface of (VMRR) versus (Servo Voltage) and (Flushing Pressure) (hold values: (pulse_ontime) = 500 n.s (pulse_offtime) = 15 μ .s (wire feed) = 2 mm/second) is presented in Fig. 12.

From this Fig. 12, it was observed that the VMRR improved when the (Servo Voltage) was raised from 35 to 45 V when the (Flushing Pressure) over 5 bar because the discharge pulses increased to the arcing, short-circuiting, and open pulses; this is indicative of an appropriate inter-electrode gap, which is very important for efficient flushing and discharge formation. Therefore, it leads to a high VMRR. Suppose the (Servo Voltage) is raised to above 45 V. In that case, the VMRR slightly decreases because there are excessive open pulses in the machining zone due to the wide separation between the electrodes [21]. Finally, it was found that if the (Flushing Pressure) is lower than 5 bars, the (Servo Voltage) does not influence the VMRR. The VMRR increases with an increase in the (Flushing Pressure) and then decreases after the (Flushing Pressure) exceeds 5 bars, as seen in Fig. Because the increase in (Flushing Pressure) enhances debris removal and improves discharge when the (Flushing Pressure) is increased to 5 bars, the debris concentration within the gap is insufficient to generate a continuous and effective discharge, resulting in a decreased VMRR [22].

The response surface of (VMRR) versus (wire feed) and (pulse_ontime) (hold values: ((pulse_offtime) = 15 μ .s (Servo Voltage) = 45 V (Flushing Pressure) = 5.25 bar)) is presented in Fig. 13.

From Fig. 13, it was observed that the VMRR increased with increasing (wire feed) value due to the rise in consumed applied current, which increases the rate of heat energy and

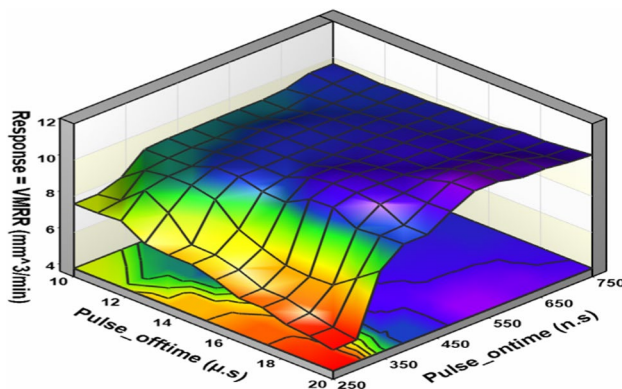


Fig. 11 Response surface of VMRR vs (pulse_ontime) and (pulse_offtime)

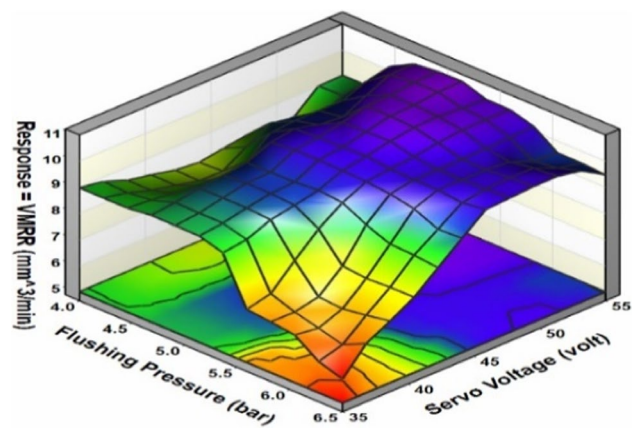


Fig. 12 Response surface of VMRR vs (Servo Voltage) and (Flushing Pressure)

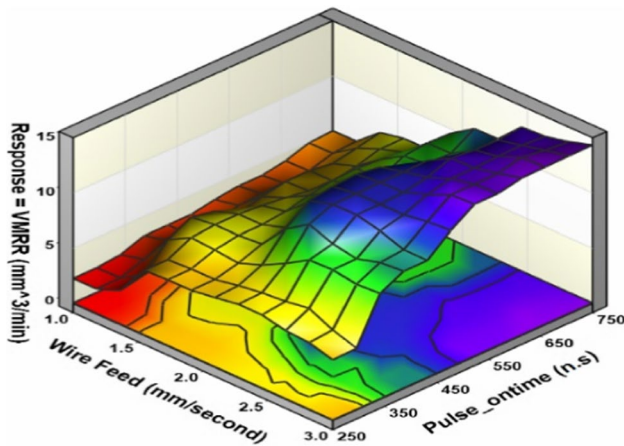


Fig. 13 Response surface of VMRR vs (wire feed) and (pulse_ontime)

hence the rate of melting and evaporation [16], and the VMRR increased with increasing (Pulse_ontime) value due to an increase in the discharge energy melting more material from the workpiece and thus increasing the VMRR [17].

5.5.2 The ANN surfaces of the (Ra) for the interaction term

The response surface of (Ra) versus (pulse_ontime) and (pulse_offtime) (hold values: (Servo Voltage)=45 V (Flushing Pressure)=5.25 bar (wire feed)=2 mm/second) is presented in Fig. 14.

From Fig. 14, it was observed that the Ra increases with an increase in (Pulse_ontime) value due to an increase in the size of craters on the machine surface as a result of increased spark intensity, resulting in poor surface quality; however, the Ra slightly decreased with an increase in (Pulse_offtime) value due to there being more time in between two

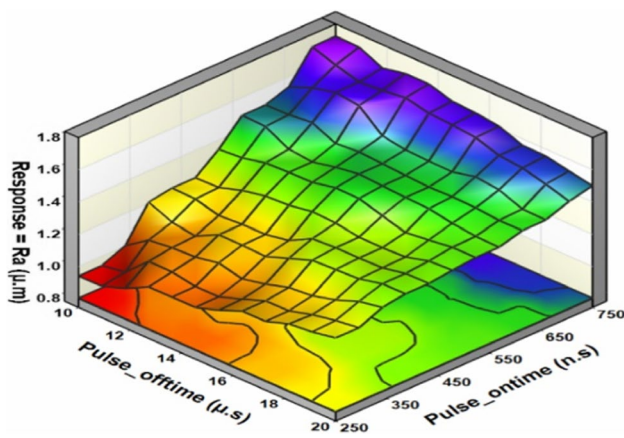


Fig. 14 Response surface of Ra vs (pulse_ontime) and (pulse_offtime)

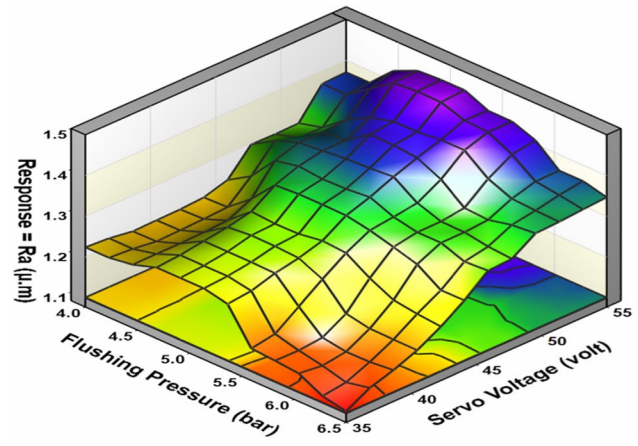


Fig. 15 Response surface of Ra vs (Servo Voltage) and (Flushing Pressure)

consecutive electrical discharges, the molten material is better flushed, thus leading to discharges, thus improving the surface quality [10].

The response surface of (Ra) versus ((Servo Voltage) and (Flushing Pressure) (hold values: (pulse_ontime)=500 n.s (pulse_offtime)=15 μ.s (wire feed)=2 mm/second) is presented in Fig. 15.

From Fig. 15, it was found that Ra goes up as (Servo Voltage) goes up because reducing the (Servo Voltage) results in a decrease in wire vibrations and deflection, which in turn leads to an improvement in surface quality characterized by a reduction in craters and cracks; however, wire breakage is observed to be higher happened with decreasing (Servo Voltage) values because the distance between the wire electrode and the workpiece is smaller, which causes wire breakage commonly occur due to slight variations. The Ra decreases with an increase in

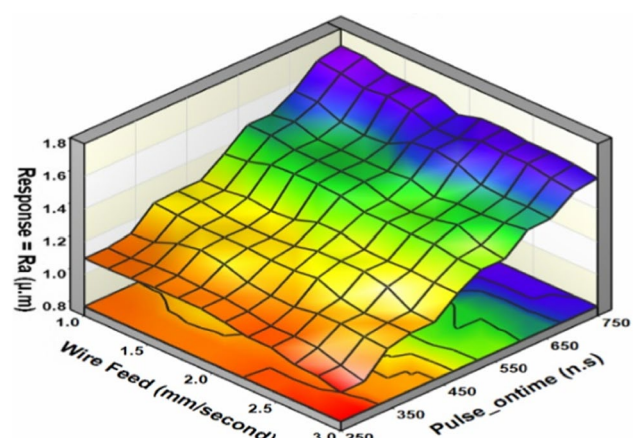
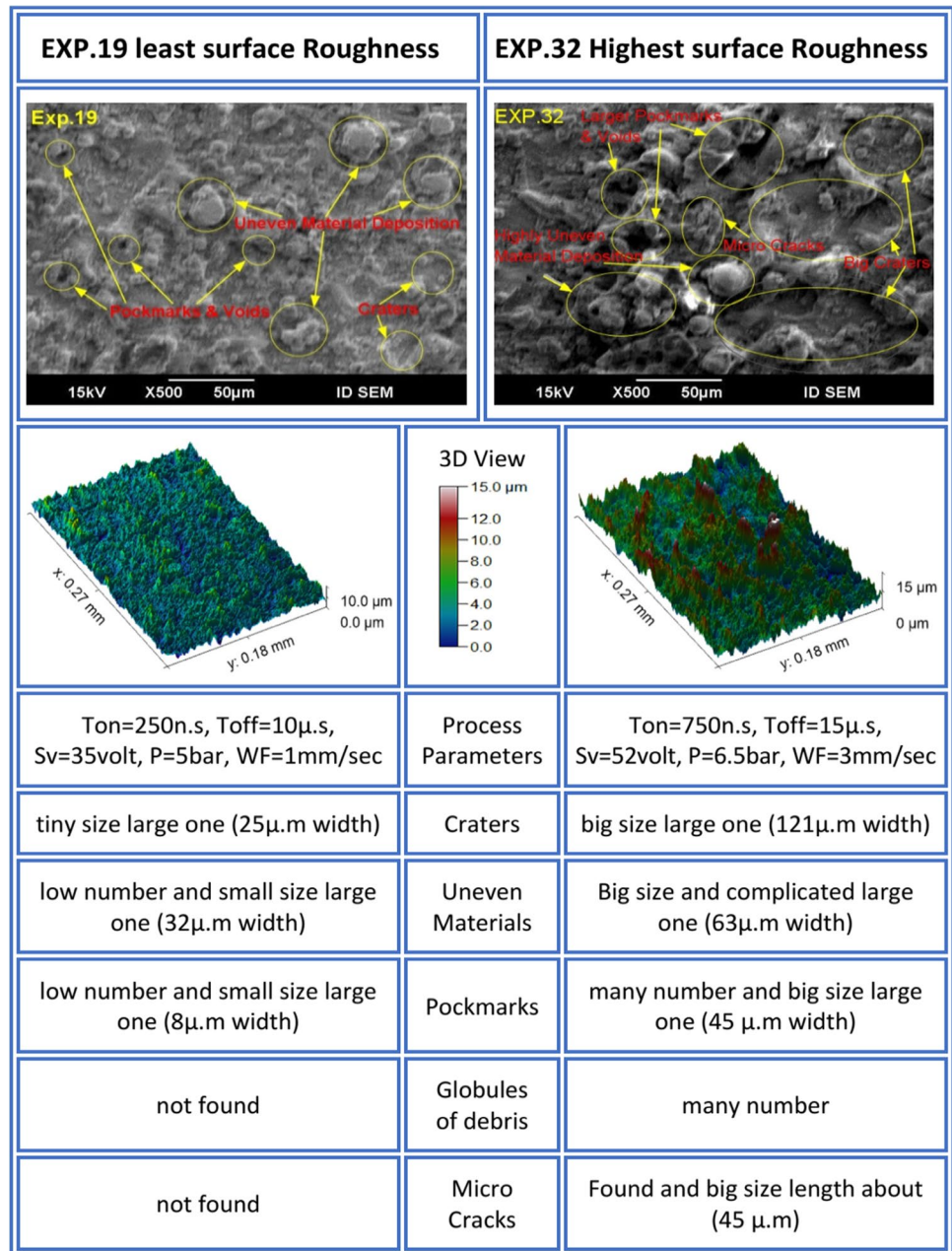


Fig. 16 Response surface of Ra vs (wire feed) and (Pulse_ontime)

Fig. 17 SEM images of the WEDMed surface and 3D images at the lowest and highest Ra values



the (Flushing Pressure), as seen in Fig. 15. Because the low (Flushing Pressure) leads to a low degree of cooling, which affects the workpiece electrode interaction area by generating more significant heat, which leads to accelerating the material evaporations; thus, a higher degree of flushing action is required to reduce the redeposition of debris on the machined surface, which ultimately improves surface quality [23].

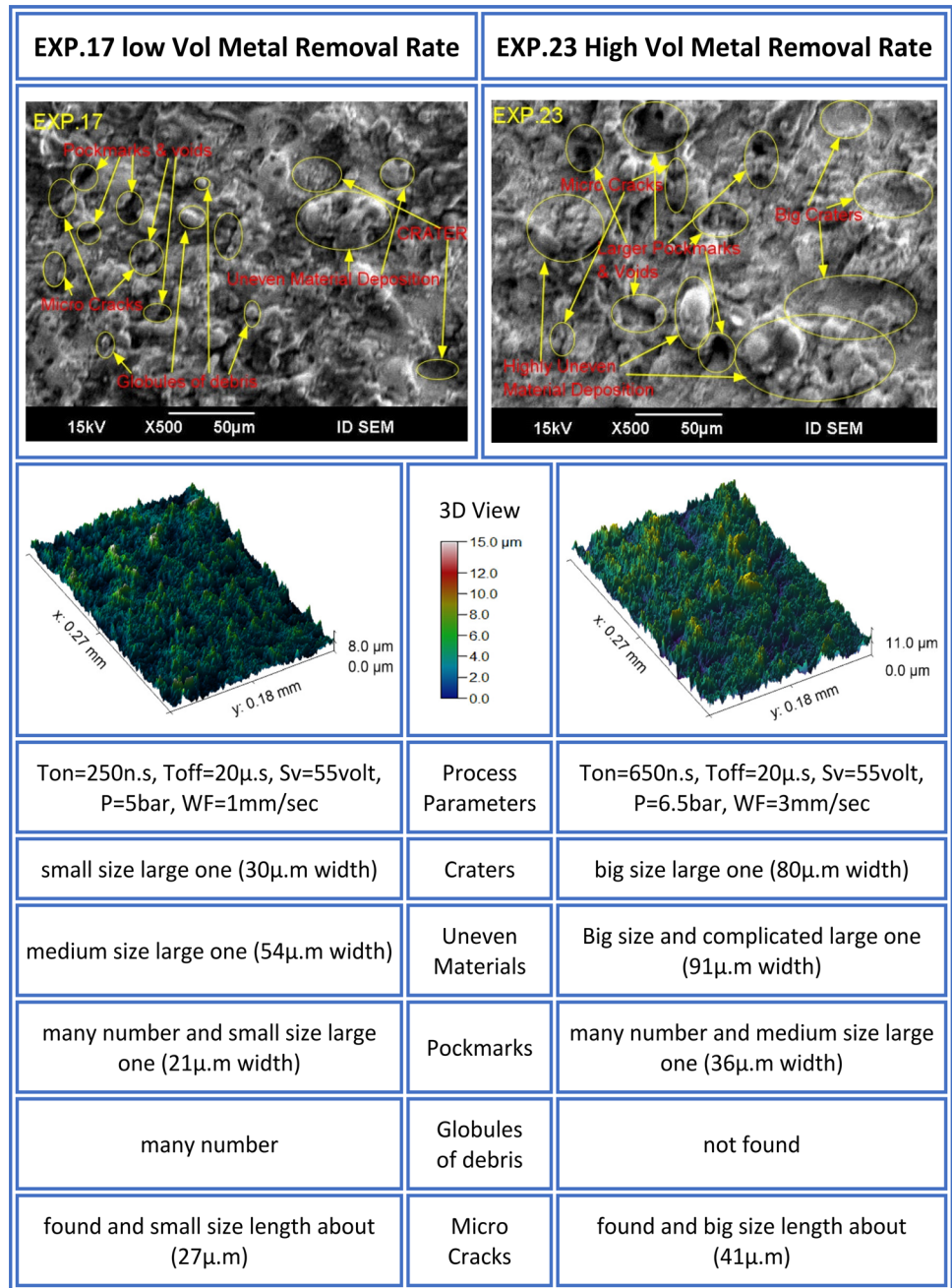
The response surface of (Ra) versus (wire feed) and (pulse_ontime) (hold values: ((pulse_offtime) = 15 µ.s (Servo Voltage) = 45 V (Flushing Pressure) = 5.25 bar)) is presented in Fig. 16.

From Fig. 16, it was observed that the Ra increases with an increase in (Pulse_ontime) value due to an increase in the size of craters on the machine surface as a result of increased spark intensity, resulting in poor surface quality [10], but the (wire feed) did not much influence the Ra.

5.6 Surface integrity analysis of machined specimens

The present investigation looked at the effect of different process parameters on the surface quality of WEDM-machined specimens. An investigation of the machined

Fig. 18 SEM images of the WEDMed surface and 3D images at the lowest and highest VMRR values

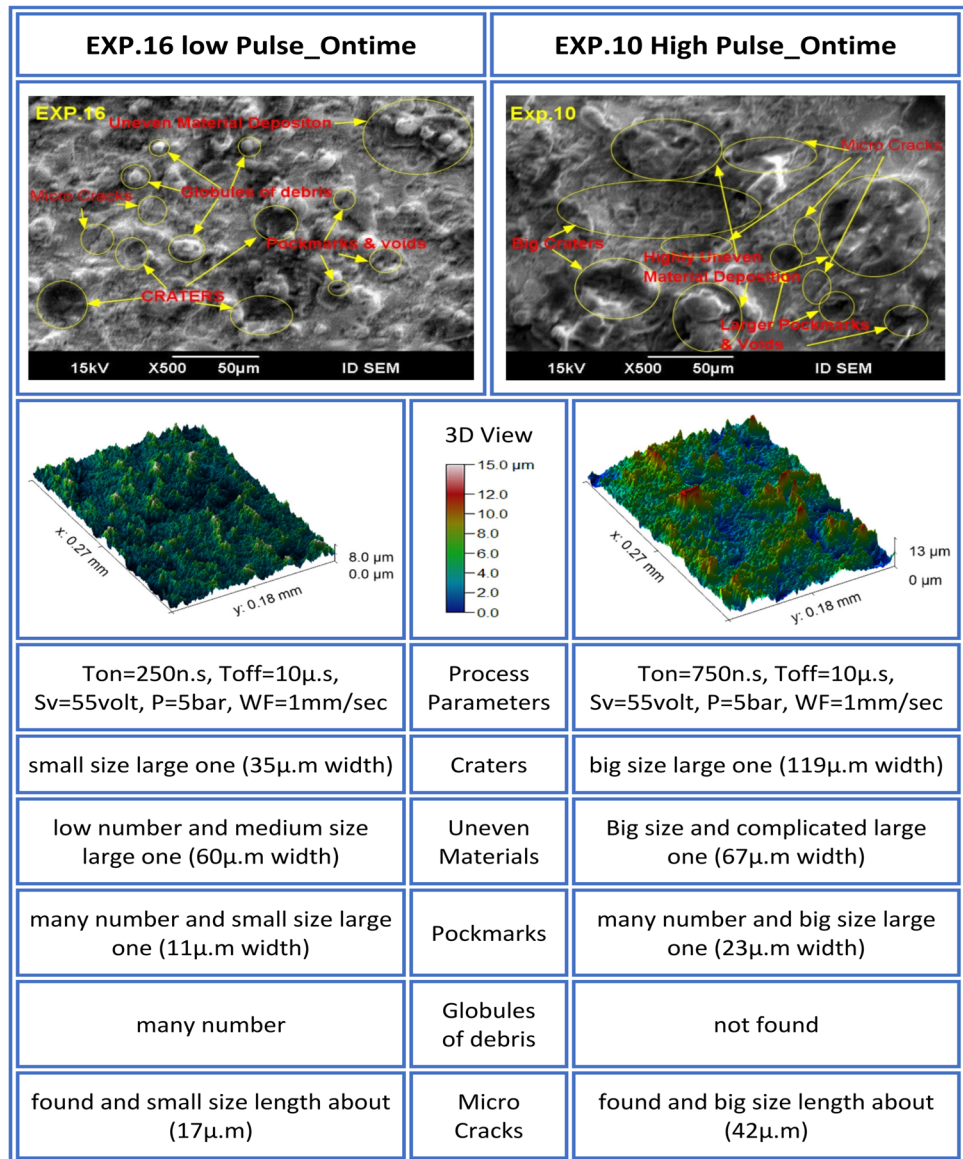


surfaces was carried out using a scanning electron microscope. Specimens were explored for a surface morphological study through the SEM technique at 500 × magnification. (SEM) micrographs and a 3D image were generated using Gwyddion 2.61 software using the SEM images and the specimen's (Ra) to better understand the surface integrity aspects.

In Fig. 17, the surfaces machined to have the lowest Ra were observed to have the fewest craters, smallest pockmarks, and most little globules of debris; no microcracks were found. However, the maximum (Ra)

is caused by numerous craters, uneven material deposition, pockmarks, and microcracks are the largest they can be. From Fig. 18, the machined surfaces with the lowest VMRR had the tiniest craters, pockmarks, and small globules of debris. Eventually, they found some microcracks. Nevertheless, the maximum VMRR shows that many craters, uneven material deposits, pockmarks, and microcracks are as giant as possible. This shows that there is a connection between VMRR and Ra. When VMRR goes down, Ra goes down, and when VMRR goes up, Ra goes up. the lowest and highest

Fig. 19 SEM images of the WEDMed surface and 3D images at the lowest and highest (Pulse_ontime) values

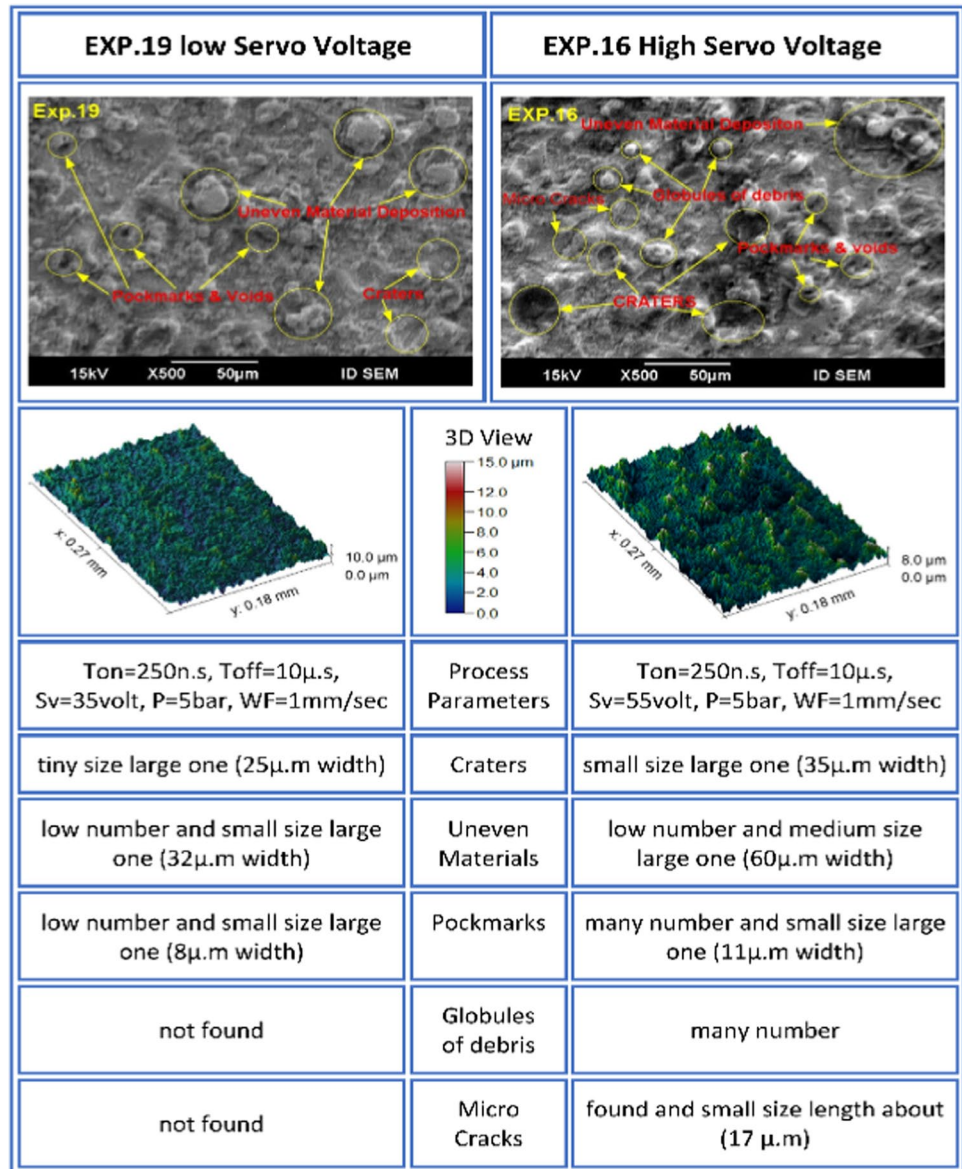


VMRR values. From Fig. 19, the machined surfaces with the low (Pulse_ontime) had the tiniest craters, many pockmarks with small sizes, and many small globules of debris. Eventually, they found some small microcracks.

Nevertheless, the high (Pulse_ontime) shows that many giant craters, extensive and complicated uneven material deposits, pockmarks, no globules of debris, and microcracks are as giant as possible. This shows that there is a connection between (Pulse_ontime) and Ra. When (Pulse_ontime) goes down, Ra goes down, and when (Pulse_ontime) goes up, Ra goes up. It can observe a rise in (Pulse_ontime) from 250 n.s to 750 n.s, enlarged pockmarks and voids, and exacerbated uneven layer deposition. Furthermore, the discharge energy emitted per spark

increases noticeably with a (Pulse_ontime) increase. More extensive and deeper craters can be formed due to greater spark intensity due to the higher discharge energy melting and vaporizing more material from the plasma channel [10]. From Fig. 20 the machined surfaces with the low (Servo Voltage) had tiny size craters, little pockmarks with small sizes, and not found any globules of debris or microcracks. Eventually, they found some small microcracks. Nevertheless, the highest (Servo Voltage) shows small craters, little and medium uneven material deposits, many tiny pockmarks, globules of debris, and small microcracks. This shows that there is a connection between (Servo Voltage) and Ra. When (Servo Voltage) goes down, Ra goes down. When (Servo Voltage) goes up, Ra goes up because reducing the (Servo Voltage)

Fig. 20 SEM images of the WEDMed surface and 3D images at the lowest and highest (Servo Voltage) values



decreases wire vibrations and deflection, improving surface quality by reducing craters and cracks [23].

5.7 Multi-objective optimization using the Pareto search algorithm for input parameters

When a company sets out to design a product with the lowest possible manufacturing costs, it needs to determine the most effective ways to cut down on wasteful practices that would otherwise use an excessive amount of time, money, and resources. Therefore, in order to achieve successful machining with a WEDM process, it is essential to optimize the machine parameter settings, which requires achieving the seemingly conflicting goal of maximizing the VMRR while minimizing the Ra. For this reason, the obtained mathematical, ANN, and ANFIS models were optimized with the

Pareto search algorithm, a very effective method that uses the pattern search algorithm’s iterative modification of point populations to find non-dominant optimal Pareto solutions for multiple objective functions. During each iteration, the population undergoes modifications to expand and enhance the Pareto front to assess the objective function values and ensure that all linear constraints and bounds are satisfied during each iteration of the pattern search. The procedures stop when small changes in the Pareto front are found, which are the non-dominant points found by the algorithm that have individuals with better fitness values, and these take a rank of 1 [24, 25].

The objective function (1).
 MaxVMRR = −MinVMRR = Fun((Pulse_ontime), (Pulse_offtime), (ServoVoltage), (Flushing Pressure), (Wire feed))

The objective function (2).

MinRa = Fun((Pulse_ontime), (Pulse_offtime), (ServoVoltage), (Flushing Pressure), (Wire feed))

Constraint_to.

250 n.sec < (Pulse_ontime) < 750 n.sec

10 μ.sec < (Pulse_offtime) < 20 μ.sec

35 volt < (Servo Voltage) < 55 volts

4 bar < (Flushing Pressure) < 6.5 bar

1 mm/sec < (wire feed) < 3 mm/sec

The Pareto search algorithm’s precise stages are described in a flowchart as illustrated in (Fig. 21).

It needs to analyze the predicted optimum response for each model to compare the three models. For VMRR, which wants to maximize it, it can see that all three models predicted different optimal combinations of process parameters. The ANFIS model predicted the highest VMRR value of 19.9 mm³/min as seen in Fig. 22 and Table 6, combining (Pulse_ontime)=750 n.s, (Pulse_offtime)=20 μ.s, (Servo Voltage)=55 V, (Flushing Pressure)=6.5 bar, and (wire feed)=3 mm/second. RSM

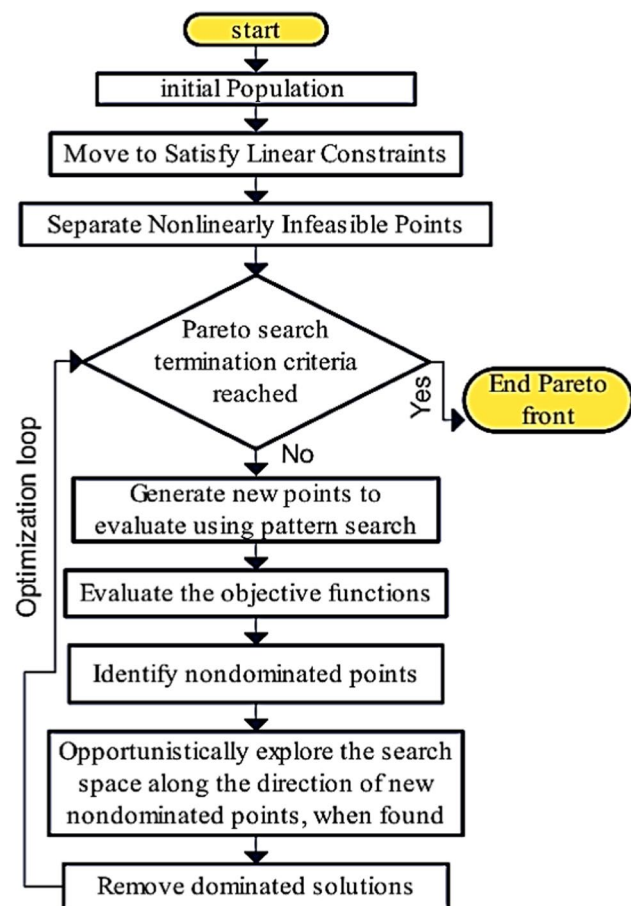


Fig. 21 Flowchart of Pareto search algorithm

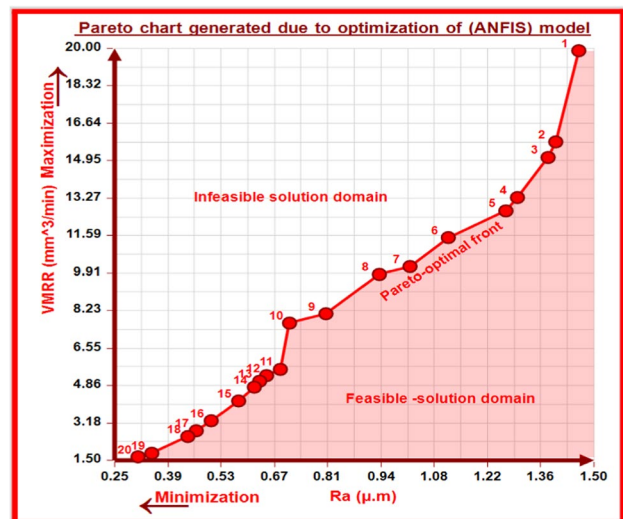


Fig. 22 Pareto front of non-dominated solutions for (ANFIS) model

predicted a slightly lower VMRR value of 19.6892 mm³/min as seen in Fig. 23 and Table 7, combining (Pulse_ontime)=734.375 n.s, (Pulse_offtime)=19.6875 μ.s, (Servo Voltage)=45.6641 V, (Flushing Pressure)=6.5 bar, and (wire feed)=3 mm/second. ANN predicted the lowest VMRR value of 18.9574 mm³/min as seen in Fig. 24 and Table 8, combining (Pulse_ontime)=750 n.s, (Pulse_offtime)=20 μ.s, (Servo Voltage)=54.375 V, (Flushing Pressure)=5.4844 bar, and (wire feed)=3 mm/second. For Ra, which wants to minimize it, it can be seen that all three models predicted different optimal combinations of process parameters. However, RSM and ANFIS predicted similar optimal combinations of process parameters for the lowest Ra value. As seen in the Fig. 25 the ANFIS model predicted the lowest Ra value of 0.311 μ.m, combining (Pulse_ontime)=250 n.s, (Pulse_offtime)=10 μ.s, (Servo Voltage)=35 V, (Flushing Pressure)=6.5 bar, and (wire feed)=3 mm/second. RSM predicted a slightly higher Ra value of 0.5813 μ.m, combining (Pulse_ontime)=250 n.s and (Pulse_offtime)=20 μ.s, (Servo Voltage)=35 V, (Flushing Pressure)=6.5 bar, and (wire feed)=3 mm/second. ANN predicted the highest Ra value of 0.7877 μ.m, combining (Pulse_ontime)=250 n.s, (Pulse_offtime)=10 μ.s, (Servo Voltage)=35 V, (Flushing Pressure)=5.2812 bar, and (wire feed)=2.375 mm/second. Finally, it was found that the ANFIS model represents the best solutions in which the VMRR maximizes and the Ra minimizes. Overall, all optimum solutions generated from the optimization of three models must be validated with employed the input parameters chosen for the actual machining process to determine which model is the most reliable for the WEDM process; unfortunately,

Table 6 Optimal combination of process parameters and non-dominated solutions for (ANFIS) model

Exp.no	The optimal combination of process parameters					Predicted optimum response	
	(Pulse_ontime) (n.s)	(Pulse_off-time) (μ .s)	(Servo Voltage) (volt)	(Flushing Pressure) (bar)	(wire feed) (mm/second)	VMRR (mm^3/min)	Ra (μ .m)
1	750	20	55	6.5	3	19.9	1.46
2	717.37	19.78	51.33	5.89	3	15.8	1.4
3	710.6875	20	50.75	5.8594	3	15.1	1.38
4	742.6875	20	48.75	6.1094	3	13.3	1.3
5	710.6875	20	48.75	6.1094	3	12.7	1.27
6	540	10	42.911	6.4572	2.992	11.5	1.12
7	531.25	10	41.25	6.5	3	10.2	1.02
8	628	10	40.6255	6.4905	2.9946	9.85	0.94
9	250	10	41	4.875	2.4219	8.09	0.801
10	260.25	10.6	40.18	5.06	3	7.67	0.706
11	471.25	10	37.5	6.5	3	5.59	0.682
12	531.25	10	35	6.5	3	5.31	0.646
13	342	10	38.5849	6.4759	2.9957	5.06	0.628
14	503.5625	10	35	6.5	3	4.79	0.614
15	468.75	10	35	6.5	3	4.17	0.573
16	408.75	10	35	6.5	3	3.28	0.502
17	375.5625	10	35	6.5	3	2.83	0.463
18	351.5625	10	35	6.5	2.9062	2.57	0.441
19	250	10	35	5.9922	2.9062	1.82	0.347
20	250	10	35	6.5	3	1.66	0.311

the abovementioned solutions are entirely theoretical and cannot be employed to select input parameters for a given process. Even so, they can assist in identifying machine

parameters that are near the solutions; however, these potential solutions could be implemented soon.

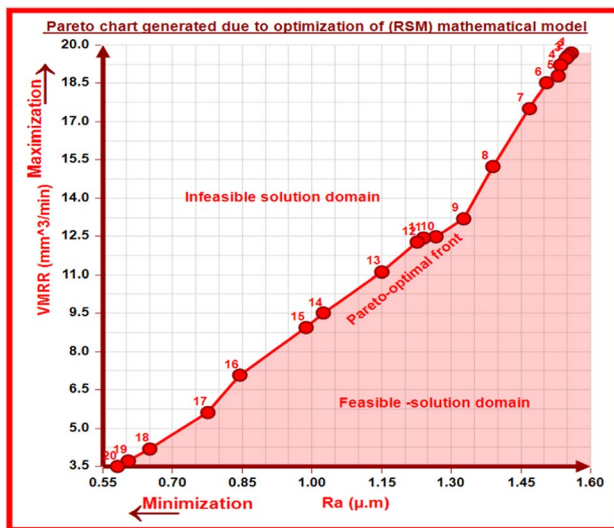


Fig. 23 Pareto front of non-dominated solutions for (RSM) mathematical model

6 Conclusion

This study aimed to construct a predictive model for machining the Inconel 718 superalloy alloy by wire electrical discharge cutting process. An I-optimal design response surface methodology was used to determine the WEDM process' experimental design. Mathematical, ANN, and ANFIS models were devised to predict performance characteristics. The effectiveness of the process optimization was determined using the Pareto search algorithm on the mathematical, ANN, and ANFIS models. The results demonstrated that the optimized process could reduce processing time and improve cost-effectiveness. The following conclusions were drawn based on the results obtained in this work.

1. The WEDM process has successfully demonstrated its capability to machine Inconel 718 alloy with an acceptable (VMRR) and (Ra) less than $1 \mu\text{m}$.

2. ANOVA results demonstrated that (wire feed) and (Pulse_ontime) were the most vital factors influencing

Table 7 Optimal combination of process parameters and non-dominated solutions for (RSM) mathematical model

Exp.no	The optimal combination of process parameters					Predicted optimum response	
	(Pulse_ontime) (n.s)	(Pulse_off-time) (μ.s)	(Servo Voltage) (volts)	(Flushing Pressure) (bar)	(wire feed) (mm/second)	VMRR (mm ³ /min)	Ra (μ.m)
1	734.375	19.6875	45.6641	6.5	3	19.6892	1.5584
2	734.375	19.6875	42.5	6.5	3	19.5873	1.5523
3	734.375	19.6875	42.5	6.5	3	19.4793	1.5471
4	734.375	19.6875	41.875	6.5	3	19.2175	1.5353
5	734.375	19.6875	41.875	6.5	3	18.7956	1.5301
6	699.375	20	42.5	6.5	3	18.5264	1.5049
7	654	20	45.6641	6.5	3	17.5125	1.4685
8	609.375	20	36.875	6.4219	3	15.241	1.3895
9	619.375	17.5	37.5	6.5	3	13.1923	1.3267
10	531.25	10	41.25	5.7188	3	12.4911	1.2668
11	609.375	10	36.875	6.4219	3	12.4415	1.2402
12	531.25	10	41.25	6.5	3	12.2814	1.2265
13	579.375	10	35	6.1875	3	11.1132	1.1503
14	471.25	10	37.5	6.5	3	9.5169	1.0245
15	448.75	10	37.5	6.5	3	8.9445	0.9872
16	408.75	10	35	6.5	3	7.0789	0.8445
17	250	10	35.7422	4.0928	3	5.6133	0.7757
18	250	10	35	5.5625	3	4.1832	0.6504
19	250	10	35	6.1875	3	3.7172	0.6043
20	250	10	35	6.5	3	3.5008	0.5813

VMRR because they contributed 50.67% and 30.67%, respectively, and the most significant factor influencing Ra is the (Pulse_ontime), which contributed 75.61%.

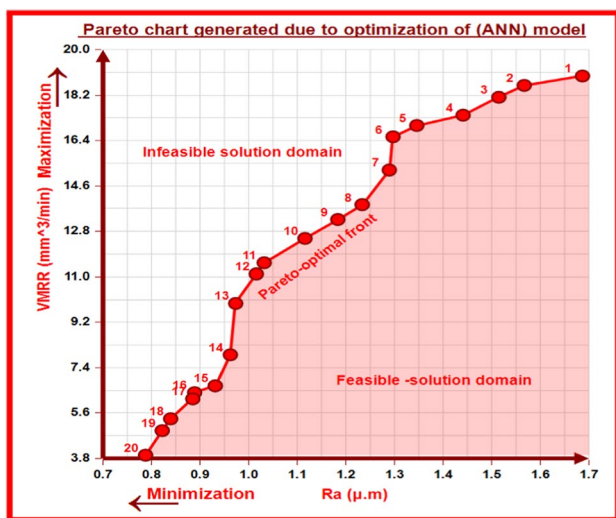


Fig. 24 Pareto front of non-dominated solutions for (ANN) model

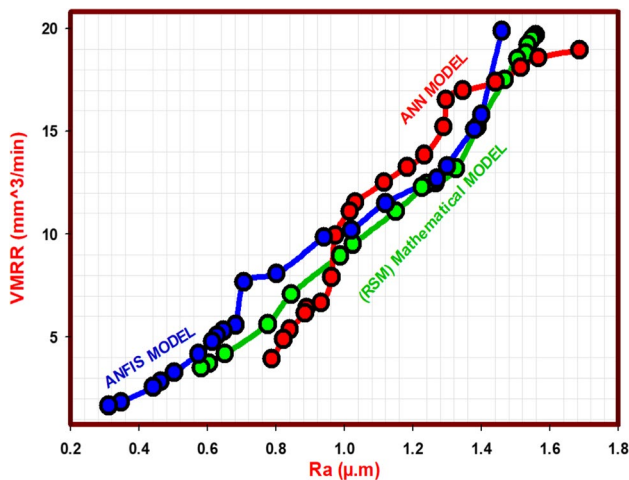
3. The I-optimal design was successfully used to establish the relationship between the performance characteristics ((VMRR) and (Ra)) and input process parameters ((Pulse_ontime), (Pulse_offtime), (Flushing Pressure), (Servo Voltage), and (wire feed)), and the results of ANOVA analysis of experimental data indicate that the RSM models for VMRR and Ra are well fitted with the experimental values, which had a total percentage error less than 6.387% for VMRR and 4.301% for Ra.

4. The ANN model was employed, utilizing the Bayesian regularization (BR) learning algorithm with 10 neurons. Additionally, the ANFIS model was utilized, with a topography structure of (2-2-3-2-2) and a Gaussian membership function. These models were used to predict DM attributes. The total percentage error of the ANN model for VMRR was 0.8738%, and for Ra, it was 2.111%, but the ANFIS model had 1.539% for VMRR and 1.069% for Ra; it was determined that the ANN and ANFIS models are more reliable and accurate than the RSM mathematical model.

5. Microstructure study revealed that WEDM machined surfaces with the lowest VMRR had the tiniest craters, pockmarks, and small globules of debris. Eventually, they found some microcracks. Nevertheless, the maximum VMRR shows

Table 8 Optimal combination of process parameters and non-dominated solutions for (ANN) model

Exp.no	The optimal combination of process parameters					Predicted optimum response	
	(Pulse_ontime) (n.s)	(Pulse_offtime) (μ .s)	(Servo Voltage) (volt)	(Flushing Pres- sure) (bar)	(wire feed) (mm/ second)	VMRR (mm ³ /min)	Ra (μ .m)
1	750	20	54.375	5.4844	3	18.9574	1.6868
2	750	20	50	5.875	3	18.5849	1.5668
3	750	20	48.75	6.0312	3	18.1145	1.5148
4	688.75	20	52.5	6.5	3	17.405	1.4412
5	628.75	20	48.75	6.0312	3	16.9955	1.3458
6	628.75	20	48.75	6.5	3	16.5483	1.2969
7	593.75	20	53.75	6.5	3	15.2273	1.2891
8	558.125	20	55	6.5	3	13.855	1.2334
9	656.25	20	36.25	5.0938	3	13.2662	1.1834
10	478.125	20	50	6.5	3	12.5165	1.1159
11	619.375	20	37.5	6.5	3	11.5522	1.0318
12	609.375	20	36.875	6.4219	3	11.1126	1.0155
13	609.375	20	35	6.4219	3	9.9493	0.973
14	579.375	16.25	35	6.1875	3	7.9117	0.962
15	296.875	10	39.375	6.1094	3	6.6798	0.9311
16	250	10	38.75	4.7812	2.375	6.4109	0.8887
17	250	10	37.5	4.625	2.2969	6.1641	0.8849
18	250	10	38	5.2812	2.375	5.373	0.8394
19	250	10	37	5.2812	2.375	4.903	0.822
20	250	10	35	5.2812	2.375	3.9303	0.7877

**Fig. 25** Comparison between Pareto front of non-dominated solutions for three models

that many craters, uneven material deposits, pockmarks, and microcracks are as giant as they can be. This shows that there is a connection between VMRR and Ra. When VMRR goes down, Ra goes down, and when VMRR goes up, Ra goes up.

Acknowledgements The author acknowledges the assistance provided by Dr. Mostafa Mahmoud Shehata, Central Metallurgical Research and Development Institute, for providing the specimen of Inconel 718 superalloy and Eng. Amr Shaalan, NEXT factory, Sadat City, Egypt, for his help in carrying out the experiments on the wire EDM machine.

Author contribution Dr. Mahmoud Hewidy supervised the experimentation and was involved in the optimization and revision of the manuscript, which improved the quality of the manuscript. Eng. Osama Salem conducted the experiment and optimized and analyzed the experimental results and manuscript preparation.

Funding Open access funding provided by The Science, Technology & Innovation Funding Authority (STDF) in cooperation with The Egyptian Knowledge Bank (EKB).

Data availability The authors confirm that the data supporting the findings of this study is available within the article.

Declarations

Ethics approval and consent to participate Not applicable.

Consent for publication Not applicable.

Conflict of interest The authors declare no competing interests.

Open Access This article is licensed under a Creative Commons Attribution 4.0 International License, which permits use, sharing, adaptation, distribution and reproduction in any medium or format, as long as you give appropriate credit to the original author(s) and the source, provide a link to the Creative Commons licence, and indicate if changes were made. The images or other third party material in this article are included in the article's Creative Commons licence, unless indicated otherwise in a credit line to the material. If material is not included in the article's Creative Commons licence and your intended use is not permitted by statutory regulation or exceeds the permitted use, you will need to obtain permission directly from the copyright holder. To view a copy of this licence, visit <http://creativecommons.org/licenses/by/4.0/>.

References

- Sharma N, Khanna R, Gupta RD (2015) WEDM process variables investigation for HSLA by response surface methodology and genetic algorithm. *Eng Sci Technol, an Int J* 18:171–177. <https://doi.org/10.1016/j.jestch.2014.11.004>
- Hewidy MS, El-Taweel TA, El-Safty MF (2005) Modelling the machining parameters of wire electrical discharge machining of Inconel 601 using RSM. *J Mater Process Technol* 169:328–336. <https://doi.org/10.1016/j.jmatprotec.2005.04.078>
- Kiran Pulidindi AP (2020) Nickel superalloy market size, by type (Alloy 600/601/602, Alloy 625, Alloy 718, Alloy 825, Alloy 925, Hastelloy C276/C22/X, Waspaloy), by shape (bar, wire, sheet & plate), by application (aerospace & defense, power generation, oil & gas, refinery, chemical). In: <https://www.gminsights.com/gmipulse>. <https://www.gminsights.com/industry-analysis/nickel-super-alloy-market>. Accessed 3 May 2023
- Mazareanu (2021) Aircraft engine market size worldwide 2019–2027, Statista. In: statista. <https://www.statista.com/statistics/1100610/aircraft-engine-market-size-worldwide/>. Accessed 3 May 2023
- Davis JR (1997) CASMIH. ASM Specialty Handbook, Heat-Resistant Materials
- Thakur A, Gangopadhyay S (2016) State-of-the-art in surface integrity in machining of nickel-based super alloys. *Int J Mach Tools Manuf* 100:25–54
- Agmell M, Bushlya V, M'Saoubi R et al (2020) Investigation of mechanical and thermal loads in pcBN tooling during machining of Inconel 718. *Int J Adv Manuf Technol* 107:1451–1462. <https://doi.org/10.1007/s00170-020-05081-8>
- Aggarwal V, Khangura SS, Garg RK (2015) Parametric modeling and optimization for wire electrical discharge machining of Inconel 718 using response surface methodology. *Int J Adv Manuf Technol* 79:31–47. <https://doi.org/10.1007/s00170-015-6797-8>
- Yusoff Y, Mohd Zain A, Sharif S et al (2018) Potential ANN prediction model for multiperformances WEDM on Inconel 718. *Neural Comput Appl* 30:2113–2127. <https://doi.org/10.1007/s00521-016-2796-4>
- Lalwani V, Sharma P, Pruncu CI, Unune DR (2020) Response surface methodology and artificial neural network-based models for predicting performance of wire electrical discharge machining of inconel 718 alloy. *Journal of Manufacturing and Materials Processing* 4. <https://doi.org/10.3390/jmmp4020044>
- Xu J, Li M, Zhong J, et al (2022) Process parameter modeling and multi-response optimization of wire electrical discharge machining NiTi shape memory alloy. *Mater Today Commun* 33. <https://doi.org/10.1016/j.mtcomm.2022.104252>
- Wan Azhar WA, Bin ST, Razib MABM (2022) Application of CANFIS for modelling and predicting multiple output performances for different materials in μ EDM. *CIRP J Manuf Sci Technol* 37:528–546. <https://doi.org/10.1016/j.cirpj.2022.02.021>
- Biswas S, Paul AR, Dhar AR et al (2023) Multi-material modeling for wire electro-discharge machining of Ni-based superalloys using hybrid neural network and stochastic optimization techniques. *CIRP J Manuf Sci Technol* 41:350–364. <https://doi.org/10.1016/j.cirpj.2022.12.005>
- Montgomery DC (2022) Design and analysis of experiments Ninth Edition. John Wiley & Sons, Inc
- Mohamed OA, Masood SH, Bhowmik JL (2017) Characterization and dynamic mechanical analysis of PC-ABS material processed by fused deposition modelling: An investigation through I-optimal response surface methodology. *Measurement (Lond)* 107:128–141. <https://doi.org/10.1016/j.measurement.2017.05.019>
- El-Taweel TA, Hewidy AM (2013) Parametric study and optimization of WEDM parameters for CK45 steel. *International Journal of Engineering Practical Research*. www.seipub.org/ijep
- El-Taweel TA (2009) Multi-response optimization of EDM with Al-Cu-Si-TiC P/M composite electrode. *Int J Adv Manuf Technol* 44:100–113. <https://doi.org/10.1007/s00170-008-1825-6>
- Dinesh Sivakumar (2023) Regression analysis using artificial neural networks. In: <https://www.scaler.com/academy/>. <https://www.scaler.com/topics/deep-learning/multiple-linear-regression/>. Accessed 3 May 2023
- Naresh C, Bose PSC, Rao CSP (2020) Artificial neural networks and adaptive neuro-fuzzy models for predicting WEDM machining responses of Nitinol alloy: comparative study. *SN Appl Sci* 2. <https://doi.org/10.1007/s42452-020-2083-y>
- Hasan MM, Saleh T, Sophian A et al (2023) Experimental modeling techniques in electrical discharge machining (EDM): A review. *Int J Adv Manuf Technol*. <https://doi.org/10.1007/s00170-023-11603-x>
- Singh MA, Joshi K, Hanzel O et al (2020) Influence of open voltage and servo voltage during Wire-EDM of silicon carbides. In: *Procedia CIRP*. Elsevier B.V., pp 285–289. <https://doi.org/10.1016/j.procir.2020.02.305>
- Tanjilul M, Ahmed A, Kumar AS, Rahman M (2018) A study on EDM debris particle size and flushing mechanism for efficient debris removal in EDM-drilling of Inconel 718. *J Mater Process Technol* 255:263–274. <https://doi.org/10.1016/j.jmatprotec.2017.12.016>
- Farooq MU, Anwar S, Kumar MS, et al (2022) A novel flushing mechanism to minimize roughness and dimensional errors during wire electric discharge machining of complex profiles on Inconel 718. *Materials* 15. <https://doi.org/10.3390/ma15207330>
- Fioriti D, Pintus S, Lutzemberger G, Poli D (2020) Economic multi-objective approach to design off-grid microgrids: A support for business decision making. *Renew Energy* 159:693–704. <https://doi.org/10.1016/j.renene.2020.05.154>
- Arthur CK, Kaunda RB (2020) A hybrid paretosearch algorithm and goal attainment method for maximizing production and reducing blast-induced ground vibration: a blast design parameter selection approach. *Mining Technology: Transactions of the Institute of Mining and Metallurgy* 151–158. <https://doi.org/10.1080/2572668.2020.1790262>

Publisher's Note Springer Nature remains neutral with regard to jurisdictional claims in published maps and institutional affiliations.